Available online at www.sciencedirect.com
SCIENCE DIRECT®
ELSEVIER
Nuclear Physics A 717 (2003) 199–213
NUCLEAR PHYSICS A
www.elsevier.com/locate/npe

Breakup of the weakly bound ^{17}F nucleus

C.A. Bertulani *, P. Danielewicz

National Superconducting Cyclotron Laboratory, Michigan State University, East Lansing, MI 48824, USA

Received 12 December 2002; received in revised form 9 January 2003; accepted 13 January 2003

Abstract

The breakup of the radioactive ^{17}F nucleus into a proton and ^{16}O is studied for the reaction $^{17}\mathrm{F} + {}^{208}\mathrm{Pb} \to \mathrm{p} + {}^{16}\mathrm{O} + {}^{208}\mathrm{Pb}$ at 65 MeV/nucleon. The possibility of using this reaction as a test case for studying dynamical Coulomb reacceleration effects is assessed. It is shown that the reaction is dominated by elastic nuclear breakup (diffraction dissociation).

PACS: 25.60.Gc; 24.10.-i

1. Introduction

The Coulomb dissociation method [1] is now a standard experimental tool as a source of information on radioactive capture processes of astrophysical interest. It can be shown that the breakup cross sections of a projectile nucleus in the Coulomb field of a target is proportional to the cross section for photo-dissociation [2]. The radiative capture cross sections can be obtained via detailed balance [1]. Thus, by measuring the Coulomb breakup of nuclear projectiles, specially at high bombarding energies ($\sim 50-200$ MeV/nucleon), one can obtain information on the radiative capture cross section of interest. This goal has indeed been achieved in numerous experiments for the study of $^{4}\mathrm{He}(\mathrm{d},\gamma)^{6}\mathrm{Li}$ [3], $^{12}\mathrm{C}(\mathrm{n},\gamma)^{13}\mathrm{C}$ [4,5], $^{11}\mathrm{C}(\mathrm{p},\gamma)^{12}\mathrm{N}$ [6], and $^{12}\mathrm{C}(\alpha,\gamma)^{16}\mathrm{O}$ [7]. More recently, this method has been used exhaustively in the study of the reaction $^{7}\mathrm{Be}(\mathrm{p},\gamma)^{8}\mathrm{B}$ [8–13], considered the most important one for the standard solar model [14].

* Corresponding author.
E-mail addresses: bertulani@nscl.msu.edu (C.A. Bertulani), danielewicz@nscl.msu.edu (P. Danielewicz).

0375-9474/03/$ – see front matter
doi:10.1016/S0375-9474(03)00640-7

Under some circumstances the relation between the Coulomb breakup measurements and the radiative capture cross sections of interest is not so straightforward. First, the radiative capture cross sections contain contributions of different electric and magnetic multipolarities which enter with different weights in the Coulomb breakup cross sections. For example, while the radiative E2 capture is very small in the reaction ^{7}Be(p, γ)^{8}B within the solar environment, its contribution is amplified in the Coulomb breakup experiments. Separation of the two contributions one depends on the structure model used for the ^{8}B nucleus [15–18]. Secondly, the nuclear contribution to the breakup has to be separated from the Coulomb breakup [17]. Finally, Coulomb reacceleration effects [19–23] have to be controlled.

The Coulomb reacceleration effects are indeed one of the main concerns in extracting the astrophysical S-factor for the reaction ^{7}Be(p, γ)^{8}B. These effects are filtered from the data by comparing them with dynamical calculations of Coulomb breakup [19–23]. Due to its relevance for the application of the Coulomb dissociation method, it is desirable to study a system where the astrophysical S-factors have been measured directly at the stellar energies and where dynamical effects can be tested. Apparently, the breakup of ^{17}F is a good candidate. The ground state of ^{17}F is loosely-bound (600 keV of separation energy into proton + ^{16}O) and its only excited state is one of the best halo states known so far in nuclear physics, being bound by only 100 keV. Besides, the S-factor for the radiative capture reaction ^{16}O(p, γ)^{17}F has been measured down to 200 keV [24]. Indeed, the breakup of the weakly bound ^{17}F well above the barrier has been considered as an important test of the dynamical breakup mechanism [25]. First theoretical analysis of this reaction has been done in Ref. [26].

In this work we study the breakup of ^{17}F into proton + ^{16}O, which would be relevant for the purpose of testing Coulomb dynamical effects by a comparison with experimental results. Thus, we do not consider the stripping of the proton from ^{17}F, or the breakup into other channels. We will only consider two breakup mechanisms: the Coulomb and the elastic nuclear breakup (or diffraction dissociation). If the proton and the ^{16}O fragments are measured in coincidence, these are the only two mechanisms of interest. We restrict our calculation to first order perturbation theory, as we want to learn about the feasibility of such experiments. We also restrict ourselves to bombarding energies of 65 MeV/nucleon, typical of laboratories like GANIL/France, GSI/Germany, NSCL/USA and RIKEN/Japan, where previous Coulomb dissociation experiments have been carried out.

We show that the Coulomb breakup cross sections are too small to allow for a reliable experimental counting rate. Also, the reaction is dominated by the elastic nuclear breakup mechanism which is more model dependent than the Coulomb breakup. The details of our calculations are presented in Section 2, where we show that a single particle model is able to explain the astrophysical S-factor for ^{16}O(p, γ)^{17}F at the lowest energies. In Section 3 we present our calculations for Coulomb breakup and in Section 4 for elastic nuclear breakup. Our conclusions are presented in Section 5.

2. Potential model for ^{17}F

In the present calculation, we treat ^{17}F as the combination of a proton and an inert ^{16}O core with spin 0. The proton–oxygen wavefunction is given by

$$\Psi_{lj}(\mathbf{r}) = \frac{u_{lj}(r)}{r} \sum_{m,m_s} \left(l\tfrac{1}{2}m_l m_s \middle| jm\right) Y_{lm_l}(\hat{\mathbf{r}})\chi_{m_s}, \tag{1}$$

where χ_{m_s} is the spinor wavefunction.

The radial wave functions $R_{lj}(r)$ are solutions of the radial Schrödinger equation for the proton-core motion with the potential

$$V(\mathbf{r}) = V_0\left[1 - F_{\text{s.o.}}(\mathbf{l}\cdot\mathbf{s})\frac{r_0}{r}\frac{d}{dr}\right]\left[1 + \exp\left(\frac{r-R}{a}\right)\right]^{-1} + V_C(r), \tag{2}$$

where

$$\begin{aligned} V_C(r) &= \frac{8e^2}{r}, \quad \text{for } r > R_C, \\ V_C(r) &= \frac{4e^2}{r}\left(3 - \frac{r^2}{R_C^2}\right), \quad \text{for } r < R_C. \end{aligned} \tag{3}$$

We use $a = 0.6$ fm, $R_C = R = 3.27$ fm, $F_{\text{s.o.}} = 0.341$ fm, and $r_0 = 1.25$ fm. For the $5/2^+$ d-wave ground state, we use the potential depth $V_0 = -49.66$ MeV, which reproduces the separation energy of 0.6 MeV. For the $1/2^+$ s-wave, we use $V_0 = -50.65$ MeV, which reproduces the separation energy of 0.1 MeV of the only excited state in ^{17}F.

The continuum wavefunctions are calculated with the same potential model parameters as the $5/2^+$ ground state. They are normalized so as to satisfy the relation

$$\langle \Psi_c | \Psi_{c'} \rangle = \delta(E_c - E_{c'})\delta_{jj'}\delta_{ll'}\delta_{mm'}, \tag{4}$$

what means, in practice, that the continuum wavefunctions $u_{Elj}(r)$ are normalized to $\sqrt{2m_{bc}/\pi\hbar^2 k}\sin(kr + \delta_{lj})$ at large r, where k is the relative momentum of the fragments b and c (oxygen and proton, respectively).

The S-factor for the direct capture from a continuum state to the bound state, with spin j_0, is given by

$$S_\lambda(E_{\text{cm}}) = \frac{(2\pi)^3(\lambda+1)}{2\lambda[(2\lambda+1)!!]^2}\frac{1}{k}\left(\frac{E_x}{\hbar c}\right)^{2\lambda+1} \exp\left[2\pi\eta(E_{\text{cm}})\right]\left|\mathcal{O}_\lambda(E_{\text{cm}}; lj; l_0 j_0)\right|^2, \tag{5}$$

where $\lambda = 1$, or 2, for E1, or E2 transitions, respectively. The electromagnetic matrix element $\mathcal{O}_\lambda(E_{\text{cm}}; lj; l_0 j_0)$ is given by

$$\begin{aligned} \mathcal{O}_\lambda(E_{\text{cm}}; lj; l_0 j_0) \;=\; & \frac{e_\lambda}{\sqrt{4\pi}}(-1)^{j_0+l_0+l-j}\left[\frac{1+(-1)^{l+l_0+\lambda}}{2}\right]\frac{\hat{\lambda}\hat{j}_0}{\hat{j}}\left(j_0\tfrac{1}{2}\lambda 0\middle| j\tfrac{1}{2}\right) \\ & \times \int u_{Elj}(r)u_{l_0 j_0}(r)r^\lambda\, dr, \end{aligned} \tag{6}$$

with the notation $\hat{j} \equiv \sqrt{2j+1}$, and $e_\lambda = Z_b e(-A_c/A_a)^\lambda + Z_c e(A_b/A_a)^\lambda$, where $a \equiv {}^{17}$F, $b \equiv {}^{16}$O and $c \equiv$ p, respectively.

In a similar fashion, the photo-absorption cross section for the reaction $\gamma + a \to b + c$ is given by

$$\sigma_\gamma^{(\lambda)}(E_{\rm cm}) = \frac{(2\pi)^3(\lambda+1)}{\lambda[(2\lambda+1)!!]^2}\left(\frac{\mu_{bc}}{\hbar^2 k}\right)\left(\frac{E_x}{\hbar c}\right)^{2\lambda-1}\left|\mathcal{O}_\lambda(E_{\rm cm}; lj; l_0 j_0)\right|^2, \tag{7}$$

while the photo-absorption cross section for the ground state to excited state transition $\gamma + a(5/2^+) \to a(1/2^+)$ is given by

$$\sigma_\gamma^{(\lambda)}(E_x) = \frac{(2\pi)^3(\lambda+1)}{\lambda[(2\lambda+1)!!]^2}\left(\frac{E_x}{\hbar c}\right)^{2\lambda-1}\left|\mathcal{O}_\lambda(l_1 j_1; l_0 j_0)\right|^2\delta(E_f - E_i - E_x), \tag{8}$$

where $|\mathcal{O}_\lambda(l_1 j_1; l_0 j_0)|$ is given by Eq. (6), with the wavefunction of the $1/2^+$ state replacing $u_{Elj}(r)$, and with $E_f - E_i = 0.5$ MeV.

In Fig. 1, we show the S-factor for the radiative capture reaction ^{16}O(p, γ)^{17}F. The data points are from Ref. [24]. We only show the low-energy part of the spectrum, up to $E_{\rm cm} = 2$ MeV. The solid curves are the result of calculations following the direct capture model as described above. The data are reasonably well described by the model, but the model overestimates the capture cross sections into the $1/2^+$ state for energies greater than 1 MeV.

In Fig. 2, we show the photo-absorption cross sections for transitions from the ground state (upper figure) and from the first excited state (lower figure) to the continuum. The curves are calculated within the direct capture model and are given as a function of the photon energy $E_\gamma = E_x = E_{\rm cm} + S_p$, where E_x is the excitation energy and S_p is the separation energy. Only shown are the E1 transition cross sections as the E2 cross sections are at least a factor of 10^3 smaller. The p-waves dominate the transitions for lower energies from the ground state to the continuum, but the f-wave contributions dominate at higher

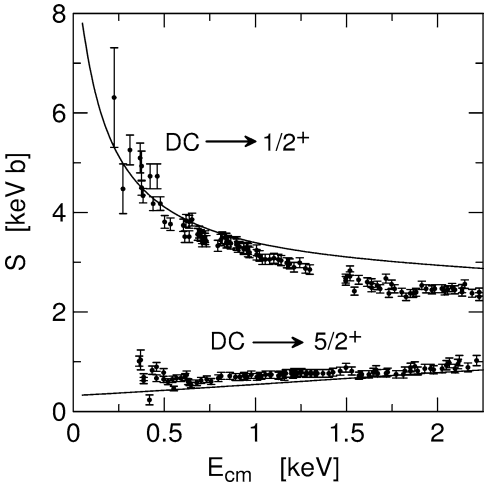

Fig. 1. S-factor for the reaction ^{16}O(p, γ)^{17}F. The upper (lower) data represent the capture to the $1/2^+$-excited ($5/2^+$-ground) state in ^{17}F. The solid curves are the result of a calculation for the direct capture with a potential model described in the text. The data are from Ref. [24].

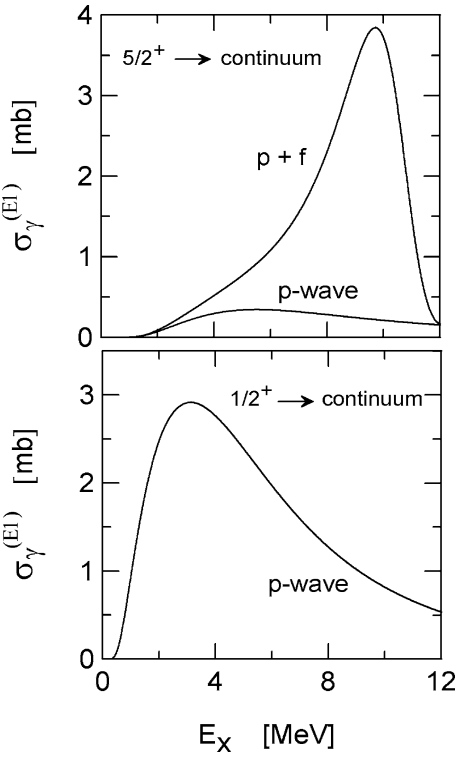

Fig. 2. The upper (lower) figure shows the photo-absorption cross section of ^{17}F for transitions from the ground (first excited) state to the continuum. The curves are calculated within the direct capture model explained in the text and are given as a function of the photon energy $E_\gamma = E_x = E_{\rm cm} + S_p$, where E_x is the excitation energy and S_p is the separation energy.

energies, of 2 MeV and above. The photo-absorption cross section for the transitions from the $1/2^+$ to the continuum is shown in the lower panel.

There is also a contribution for the excitation of the $1/2^+$ bound-state from the ground state. This contribution was calculated by using Eq. (8). The cross section value integrated over the line is $\int \sigma_\gamma^{(5/2^+\to 1/2^+)}(E_x)\,dE_x = 7\times 10^{-6}$ mb MeV. The result can be translated into a B(E2)-value for the down transition $B(\mathrm{E2};\, 1/2^+ \to 5/2^+) = 61.5\, e^2\,\mathrm{fm}^2$, which is rather close to the experimental value of $66.4 \pm 1.4\, e^2\,\mathrm{fm}^2$ [27]. This is indeed verified in more elaborate calculations [28], the reason being that the loosely-bound states in ^{17}F have a small overlap with the core, thus leading to a small core polarization. Single particle states are thus a good approximation for these states.

One observes from Fig. 2 that the photo-absorption cross sections have maxima at rather high energies, ($E_{\rm max} \sim 10$ MeV for the g.s. and $E_{\rm max} \sim 3$ MeV for the excited state) in contrast to the photo-absorption cross sections of neutron halo nuclei [29]. As explained in Ref. [29], the photo dissociation cross section peaks at an energy of about twice the binding energy of neutron halo states. The cause of the peaks moving towards the higher energies is the Coulomb barrier which produces a reduction of the overlap integral in Eq. (6). The

result is an effective separation energy that is much larger than in neutron halo systems with the same separation energies.

3. Coulomb breakup

Since there are no data for the elastic scattering of ^{17}F on Pb targets at high bombarding energies, we construct an optical potential using an effective interaction of the M3Y type [31,32] modified so as to reproduce the energy dependence of total reaction cross sections, i.e. [32],

$$t(E,s) = -i\frac{\hbar v}{2t_0}\sigma_{\rm NN}(E_{\rm lab})\big[1 - i\alpha(E_{\rm lab})\big]t(s), \tag{9}$$

where $t_0 = 421$ MeV fm^3 is the volume integral of the M3Y interaction $t(s)$, s is the nucleon–nucleon separation distance, v is the projectile velocity, $\sigma_{\rm NN}$ is the nucleon–nucleon cross section, and α is the real-to-imaginary ratio of the forward nucleon–nucleon scattering amplitude. At 65 MeV/nucleon, we use $\sigma_{\rm NN} = 82$ fm^2 and $\alpha = 0.96$.

The optical potential is given by

$$U(E_{\rm lab}, \mathbf{R}) = \int d^3r_1\, d^3r_2\, \rho_P(\mathbf{r}_1)\rho_T(\mathbf{r}_2)t(E_{\rm lab}, s), \tag{10}$$

where $\mathbf{s} = \mathbf{R} + \mathbf{r}_2 - \mathbf{r}_1$, and ρ_T (ρ_P) is the ground state density of the target (projectile). For the proton, we use a Gaussian density characterized by a width of 0.7 fm. For ^{16}O and ^{208}Pb we use the matter densities tabulated in Ref. [33].

Following Refs. [34,35], the Coulomb amplitude for E1 transitions is given by

$$\begin{aligned} f_{\rm E1}^{(jm,j_0m_0)} &= 2\sqrt{\frac{2\pi}{3}}\, i^{\mu}\frac{Z_T e\mu_{PT}}{\hbar^2}\left(\frac{E_x}{\hbar v}\right)\big\langle j_0 m_0 1(m-m_0)\big|jm\big\rangle \\ &\quad\times \mathcal{O}_1(E_{\rm cm}; lj; l_0j_0)g_\mu(\gamma)\Omega_\mu(q), \end{aligned} \tag{11}$$

where μ_{PT} is the reduced mass of the target + projectile, v is their relative velocity, $\gamma = (1 - v^2/c^2)^{-1/2}$, and

$$\Omega_\mu(q) = \int_0^\infty db\, bJ_\mu(qb)K_\mu\left(\frac{E_x b}{\gamma\hbar v}\right)\exp\big[i\chi(b)\big], \tag{12}$$

where $q = 2p_{\rm cm}\sin(\theta/2)$, $p_{\rm cm}$ is the center of mass bombarding momentum and θ is the scattering angle. The function $J_\mu(K_\mu)$ is the cylindrical (modified) Bessel function of order μ. The functions $g_\mu(\gamma)$ are given by

$$g_0 = \frac{\sqrt{2}}{\gamma}, \qquad g_1 = -g_{-1} = i. \tag{13}$$

The eikonal phase, $\chi(b)$, is given by

$$\chi(b) = 2\eta\ln(kb) - \frac{1}{\hbar v}\int_{-\infty}^{\infty} dz\, U_{\rm opt}(R), \tag{14}$$

where $\eta = Z_P Z_T e^2/\hbar v$, $\hbar k = p_{\rm cm}$ is the center of mass momentum, and $R = \sqrt{b^2+z^2}$. The optical potential, $U_{\rm opt}$, in the above equation is given by Eq. (10).

In a similar fashion, the E2 transition amplitudes are given by

$$f_{\rm E2}^{(jm,j_0m_0)} = 2\sqrt{\frac{\pi}{30}}\, i^{\mu}\frac{Z_T e\mu_{PT}}{\hbar^2}\left(\frac{E_x}{\hbar v}\right)^2 \langle j_0 m_0 2\mu | jm\rangle \times \mathcal{O}_2(E_{\rm cm}; lj; l_0 j_0) h_\mu(\gamma)\Omega_\mu(q), \tag{15}$$

where $\mu = m - m_0$, and

$$h_0 = i\frac{\sqrt{6}}{\gamma}, \qquad h_1 = -h_{-1} = -\left(1+\frac{1}{\gamma^2}\right), \qquad h_2 = h_{-2} = -i\frac{1}{\gamma}. \tag{16}$$

The cross section for Coulomb excitation of a state with angular momentum j and excitation energy E_x is obtained by averaging (and summing) over the initial (final) angular momentum projections:

$$\frac{d^2\sigma_C^{(lj)}}{d\Omega\, dE_x} = \frac{1}{2j_0+1}\sum_{m_0,m}\left|f_{\rm E1}^{(jm,j_0m_0)} + f_{\rm E2}^{(jm,j_0m_0)}\right|^2. \tag{17}$$

The E1 and E2 amplitudes do not interfere in the cross section after summation over angular momentum projections. This can easily be seen using the orthonormality condition of the Clebsh–Gordan coefficients:

$$\sum_{m_0,m}\langle j_0 m_0 2\mu | jm\rangle\langle j_0 m_0 1\mu | jm\rangle = 0. \tag{18}$$

Thus, Eq. (17) is just a sum of cross sections for the E1 and E2 excitations separately:

$$\frac{d^2\sigma_C^{(lj)}}{d\Omega\, dE_x} = \frac{d^2\sigma_{\rm E1}^{(lj)}}{d\Omega\, dE_x} + \frac{d^2\sigma_{\rm E2}^{(lj)}}{d\Omega\, dE_x} = \frac{n_{\rm E1}(E_x,\theta)}{E_x}\sigma_\gamma^{(\lambda j)}(E_x) + \frac{n_{\rm E2}(E_x,\theta)}{E_x}\sigma_\gamma^{(\lambda j)}(E_x), \tag{19}$$

where the virtual photon numbers $n_{\rm E1}$ and $n_{\rm E2}$ are given by

$$n_{\rm E1}(E_x,\theta) = \frac{Z_T^2\alpha}{\pi^2}\left(\frac{c}{v}\right)^2\left[\zeta_1(\omega) + \frac{1}{\gamma^2}\zeta_0(\omega)\right],$$
$$n_{\rm E2}(E_x,\theta) = \frac{Z_T^2\alpha}{\pi^2}\left(\frac{c}{v}\right)^4\left[\frac{1}{\gamma^2}\zeta_2(\omega) + \left(1+\frac{1}{\gamma^2}\right)^2\zeta_1(\omega) + \frac{3}{\gamma^2}\zeta_0(\omega)\right], \tag{20}$$

with $\alpha = 1/137$ and

$$\zeta_\mu(\omega) = 2\pi\left(\frac{\omega}{\gamma v}\right)^2\int db\, b K_\mu^2\left(\frac{\omega b}{\gamma v}\right)\exp\bigl[-2\,\mathrm{Im}\,\chi(b)\bigr]. \tag{21}$$

Fig. 3 shows the Coulomb breakup cross section $d\sigma/dE$ (in mb/MeV) for the reaction ^{17}F(65 MeV/nucleon) + Pb $\rightarrow$ ^{16}O + p + Pb, as a function of the proton–^{16}O relative energy, in MeV. The smaller panel on the upper right corner of the figure shows the cross

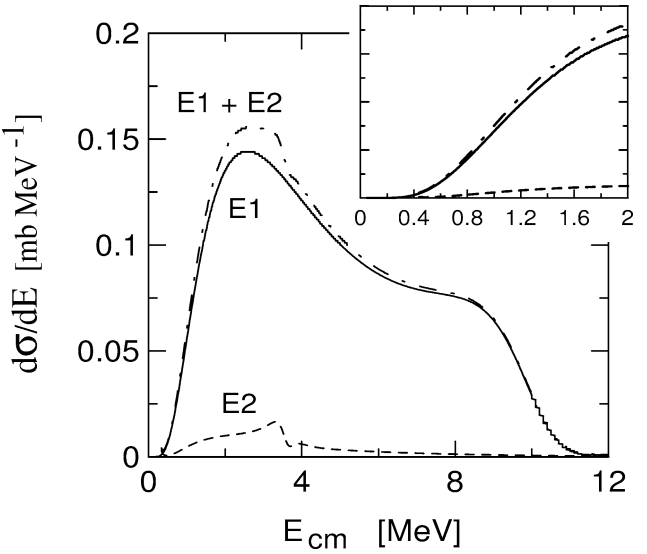

Fig. 3. Coulomb breakup cross section $d\sigma/dE$ (in mb/MeV) for the reaction ^{17}F(65 MeV/nucleon) + Pb $\rightarrow$ ^{16}O + p + Pb, as a function of the proton–^{16}O relative energy, in MeV.

section at energies up to $E_{\rm cm} = 2$ MeV. One sees that the E1 breakup mode is dominant at all energies.

Although the E2 contribution to the photo-dissociation cross section is very small it is amplified in the Coulomb dissociation due to the large abundance of E2 photons at the bombarding energy considered [30]. However, the E2 contribution to $d\sigma/dE$ is only relevant at $E_{\rm cm} \sim 3$ MeV where the cross section has a peak. We also note that this cross section is about a factor 10^3 smaller than the Coulomb breakup cross section for the reaction ^{8}B + Pb $\rightarrow$ ^{7}Be + p + Pb at similar bombarding energies [8–13]. Thus, it is much more likely that the breakup is dominated by the nuclear interaction in this case. We will demonstrate this to be indeed the case in the next section.

The angle integrated cross sections for ground state to continuum transitions are $\sigma_{\rm E1} = 0.88$ mb, $\sigma_{\rm E2} = 0.054$ mb and $\sigma_{\rm total} = 0.94$ mb, respectively. This should be compared to the cross section for the excitation of the $1/2^+$ state which is 0.33 mb. These cross sections are small and hard to measure with reliable accuracy at present laboratory facilities. Also, since the strength of the Coulomb breakup is much reduced for ^{17}F as compared to the breakup of ^{8}B projectiles, one also expects that higher order effects, which play a role in the breakup of ^{8}B, become smaller in the case of ^{17}F breakup.

4. Nuclear breakup

The nuclear breakup is due to the nuclear interaction

$$U(\mathbf{R}, \mathbf{r}) = U_{\rm p}(\mathbf{r}_{\rm p}) + U_{\rm O}(\mathbf{r}_{\rm O}) - U_{\rm F}(\mathbf{R}), \tag{22}$$

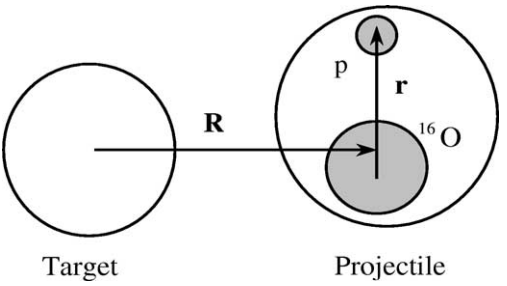

Fig. 4. Coordinates used in the text to describe the ^{17}F breakup.

where $U_{\rm p}(\mathbf{r}_{\rm p})$, $U_{\rm O}(\mathbf{r}_{\rm O})$, and $U_{\rm F}(\mathbf{R})$ are the optical potentials for the scattering of the proton, oxygen, and fluorine, off the target, respectively. The vectors $\mathbf{r}_{\rm p}$, $\mathbf{r}_{\rm O}$, and $\mathbf{R}$ are their respective coordinates relative to the target (see Fig. 4). The fluorine-projectile potential is only responsible for the center of mass scattering and does not influence the ^{17}F breakup.

The DWBA matrix element for the breakup, under the assumption of spherically symmetric potentials, is given by

$$T_{\rm N} = \left\langle \Phi^{(-)}(\mathbf{R})\Psi_E(\mathbf{r})\middle| U_{\rm p}(|\mathbf{R}-\beta_1\mathbf{r}|) + U_{\rm O}(|\mathbf{R}-\beta_2\mathbf{r}|)\middle|\Psi_{\rm g.s.}(\mathbf{r})\Phi^{(+)}(\mathbf{R})\right\rangle, \tag{23}$$

where $\mathbf{r}$ denotes the relative coordinate between the proton and the oxygen core in ^{17}F, $\Phi^{(-)}(\mathbf{R})$ is the ingoing and $\Phi^{(+)}(\mathbf{R})$ is the outgoing center of mass (c.m.) scattering wavefunction, and where $\beta_1 = 16/17$ and $\beta_2 = -1/17$ (see Fig. 4).

For the c.m. scattering at high energies one can use the eikonal approximation which implies

$$\Phi^{(-)*}(\mathbf{R})\Phi^{(+)}(\mathbf{R}) = \exp\bigl[-i\,\mathbf{q}\cdot\mathbf{R} + i\,\chi(b)\bigr], \tag{24}$$

where $\mathbf{q} = \mathbf{k}' - \mathbf{k}$ is the momentum transfer to the c.m. and $\chi(b)$ is the eikonal phase for the c.m. scattering, given by Eq. (14). Since the momentum transfer is small compared to the total projectile momentum, we can use $q = 2p_{\rm cm}\sin(\theta/2)$, where θ is the scattering angle.

It is appropriate to expand the potentials $U_i(|\mathbf{R}-\beta_i\mathbf{r}|)$ into multipoles to exploit the spherical symmetry of the states in ^{17}F. One has then

$$\begin{aligned} U_i(|\mathbf{R}-\beta_i\mathbf{r}|) &= \sum_\lambda \mathcal{F}_\lambda^{(i)}(r,R)\,P_\lambda(\cos\theta) \\ &= \sum_{\lambda\mu}\frac{4\pi}{2\lambda+1}\mathcal{F}_\lambda^{(i)}(r,R)Y_{\lambda\mu}(\widehat{\mathbf{R}})Y^*_{\lambda\mu}(\hat{\mathbf{r}}), \end{aligned} \tag{25}$$

where

$$\mathcal{F}_\lambda^{(i)}(r,R) = \frac{2\lambda+1}{2}\int_{-1}^{1} d\xi\,P_\lambda(\xi)U_i\left(\sqrt{\beta_i^2 r^2 + R^2 - 2\beta_i r R\xi}\right), \tag{26}$$

and $P_\lambda(\xi)$ are the Legendre polynomials.

Employing Eq. (1) and the angular momentum algebra, we get for the case of excitation into a continuum state with angular momentum quantum numbers jm

$$T_{\rm N}^{(j_0 m_0;\, jm;\lambda)} = -i\sqrt{4\pi}\,(-1)^{-m_0}\langle j_0 m_0 \lambda\mu | jm\rangle \left[\frac{1+(-1)^{l+l_0+\lambda}}{2}\right] \times \frac{\hat{j}_0\hat{j}}{\hat{\lambda}^3}\big(j_0\tfrac{1}{2}\lambda 0\big|\, j\tfrac{1}{2}\big)\int_0^\infty dr\, u_{Elj}(r) u_{l_0 j_0}(r)\mathcal{G}_{\lambda\mu}(r,\mathbf{q}), \tag{27}$$

where $\mu = m - m_0$, the function $\mathcal{G}$ is

$$\mathcal{G}_{\lambda\mu}(r,\mathbf{q}) = \int d^3R \exp\big[-i\mathbf{q}\cdot\mathbf{R} + i\chi(b)\big]\mathcal{F}_\lambda(r,R)Y^*_{\lambda\mu}(\widehat{\mathbf{R}}) = 4\pi i^\lambda Y^*_{\lambda\mu}(\hat{\mathbf{q}})\int_0^\infty dR\, R^2 j_\lambda(qR)\,\mathcal{F}_\lambda(r,R)\exp\big[i\chi(R)\big], \tag{28}$$

and $\mathcal{F}_\lambda(r,R) = \sum_i \mathcal{F}^{(i)}_\lambda(r,R)$.

In obtaining the last result in the equation above we have used the approximation $\chi(b) \sim \chi(R)$ which is here well justified, since the breakup occurs at the contact surface between the two nuclei, at which point $z \sim 0$. Another simplifying approximation is to assume that the momentum transfer to the c.m. is mostly in the perpendicular direction, following the spirit of the eikonal approximation. Thus, we make the substitution $Y^*_{\lambda\mu}(\hat{\mathbf{q}}) \to Y^*_{\lambda\mu}(\pi/2)$, and Eq. (28) becomes

$$\mathcal{G}_{\lambda\mu}(r,\mathbf{q}) = i^\lambda(-1)^{(\lambda+\mu)/2}\left[\frac{1+(-1)^{\lambda+\mu}}{2}\right]\left[\frac{1+(-1)^{l+l_0+\lambda}}{2}\right] \times \frac{\sqrt{4\pi(2\lambda+1)(\lambda-\mu)!(\lambda+\mu)!}}{(\lambda-\mu)!!(\lambda+\mu)!!} \times \int_0^\infty dR\, R^2 j_\lambda(qR)\mathcal{F}_\lambda(r,R)\exp\big[i\chi(R)\big]. \tag{29}$$

The (elastic) nuclear breakup cross scattering amplitude is given by ($\lambda+\mu =$ even)

$$f_{\rm N}^{(j_0 m_0;\, jm;\lambda)}(\theta) = -\frac{\mu_{PT}}{2\pi\hbar^2}T_{\rm N}^{(j_0 m_0;\, jm;\lambda)} = i\frac{2\mu_{PT}}{\hbar^2}(-1)^{-m_0+(\lambda+\mu)/2}\langle j_0 m_0\lambda\mu|jm\rangle\left[\frac{1+(-1)^{\lambda+\mu}}{2}\right]\frac{\sqrt{(\lambda-\mu)!(\lambda+\mu)!}}{(\lambda-\mu)!!(\lambda+\mu)!!} \times \int dR\, R^2 j_\lambda(qR)\exp\big[i\chi(R)\big]\,\mathcal{O}^{(N)}_\lambda(E_{\rm cm};R;lj;l_0 j_0), \tag{30}$$

where

$$\mathcal{O}^{(N)}_\lambda(E_{\rm cm};R;lj;l_0 j_0) = \left[\frac{1+(-1)^{l+l_0+\lambda}}{2}\right]\frac{\hat{j}_0\hat{j}}{\hat{\lambda}^2}\big(j_0\tfrac{1}{2}\lambda 0\big|\, j\tfrac{1}{2}\big) \times \int_0^\infty dr\, u_{Elj}(r)u_{l_0 j_0}(r)\,\mathcal{F}_\lambda(r,R), \tag{31}$$

and the cross section is

$$\begin{aligned}\frac{d\sigma_{\rm N}^{(lj)}}{d\Omega\, dE} &= \frac{1}{2j_0+1}\sum_{m_0,m,\lambda}\left|f_{\rm N}^{(j_0m_0;\,jm;\lambda)}(\theta)\right|^2 \\ &= \left(\frac{2\mu_{PT}}{\hbar^2}\right)^2\sum_{\lambda}C(\lambda j j_0) \\ &\quad\times\left|\int dR\; R^2 j_\lambda(qR)\exp\bigl[i\chi(R)\bigr]\mathcal{O}_\lambda^{(N)}(E_{\rm cm};\,R;\,lj;\,l_0j_0)\right|^2 \\ &= \left(\frac{2\mu_{PT}}{\hbar^2}\right)^2 \\ &\quad\times\sum_{\lambda}\left|\int dR\, R^2 j_\lambda(qR)\exp\bigl[i\chi(R)\bigr]\widetilde{\mathcal{O}}_\lambda^{(N)}(E_{\rm cm};\,R;\,lj;\,l_0j_0)\right|^2, \end{aligned} \tag{32}$$

with

$$C(\lambda j j_0)=\frac{1}{2j_0+1}\sum_{\substack{m_0,m\\(\lambda+\mu=\text{even})}}\langle j_0m_0\lambda\mu|jm\rangle^2\frac{(\lambda-\mu)!(\lambda+\mu)!}{[(\lambda-\mu)!!(\lambda+\mu)!!]^2},$$

and

$$\widetilde{\mathcal{O}}_\lambda^{(N)}(E_{\rm cm};\,R;\,lj;\,l_0j_0)=\sqrt{C(\lambda j j_0)}\,\mathcal{O}_\lambda^{(N)}(E_{\rm cm};\,R;\,lj;\,l_0j_0). \tag{33}$$

In Fig. 5, we plot the real part of the overlap function $\widetilde{\mathcal{O}}_\lambda^{(N)}$ as a function of R, for $\lambda=0$, 1 and 2, at $E_{\rm cm}=1$ MeV. For $\lambda=0$, only the transition from the $\mathrm{d}\frac{5}{2}$ ground state to the $\mathrm{d}\frac{5}{2}$ continuum states is accounted for. For $\lambda=1$, transitions to the $\mathrm{p}\frac{3}{2}$, $\mathrm{f}\frac{5}{2}$, and $\mathrm{f}\frac{7}{2}$ are included, while for $\lambda=2$ the transitions to the $\mathrm{s}\frac{1}{2}$, $\mathrm{d}\frac{3}{2}$ and $\mathrm{d}\frac{5}{2}$ were considered. One observes that the overlap function $\widetilde{\mathcal{O}}_\lambda^{(N)}$ extends to large distances R between the c.m. of the two nuclei (especially for $\lambda=1,2$). The low distance part of this function is not relevant, due to the nuclear absorption at low impact parameters (included in the factor $\exp[i\chi(R)]$ of Eq. (32)). The imaginary part of $\widetilde{\mathcal{O}}_\lambda^{(N)}$ has a similar behavior as the real part.

In Fig. 6, we plot the elastic nuclear breakup cross section as a function of energy, obtained by integrating Eq. (32) over angles. The dashed, solid and dashed-dotted curves represent the contributions of the $\lambda=0$, 1, and 2 multipolarities, respectively. One observes that the nuclear breakup cross sections are at least two orders of magnitude larger than the Coulomb cross sections, as displayed in Fig. 3. The elastic nuclear breakup also leads to fragments with larger relative energies. We have noticed this result does not vary appreciably with the bombarding energy.

In Fig. 7, we plot the total (solid curve) breakup cross section as a function of the relative energy of the proton $+\,^{16}$O. The cross section includes elastic nuclear and Coulomb breakup and Coulomb–nuclear interference. The figure is shown for the energies of interest for astrophysics, up to 2 MeV. The dashed curve is for the elastic nuclear breakup only. One

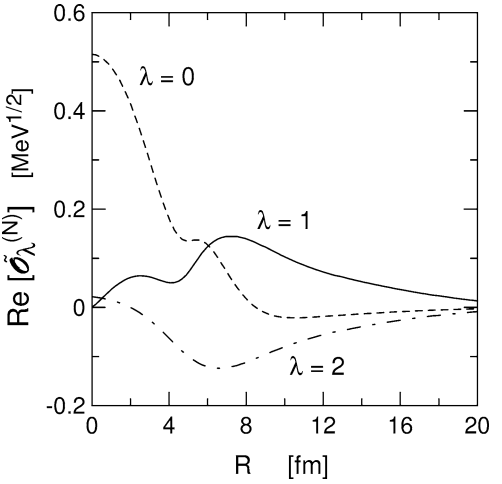

Fig. 5. The overlap function $\widetilde{\mathcal{O}}_\lambda^{(N)}$, defined by Eqs. (31) and (33), as a function of R, for $\lambda = 0$, 1 and 2, and for excitation energy $E_x = 1.5$ MeV.

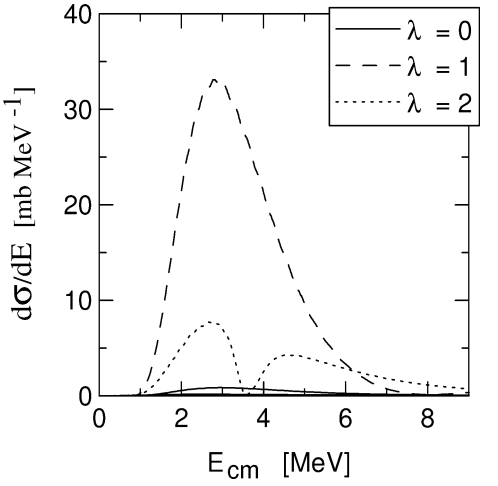

Fig. 6. Elastic nuclear breakup cross section $d\sigma/dE$ (in mb/MeV) for the reaction ^{17}F(65 MeV/nucleon) + Pb $\rightarrow$ ^{16}O + p + Pb, as a function of the proton–^{16}O relative energy, in MeV.

clearly sees that the Coulomb breakup accounts only for a tiny fraction of the total breakup cross section.

Finally, in Fig. 8 the angular distribution of the Coulomb and nuclear breakup modes are compared. The distribution was obtained by integration of the double differential cross section, Eq. (32), over energy. One observes that even at the very forward angles where the Coulomb excitation is by comparison strongest, the nuclear breakup dominate.

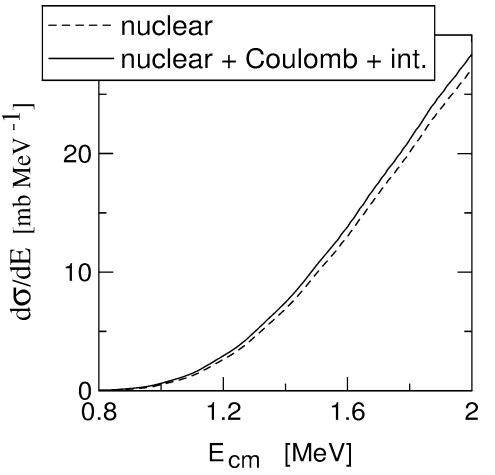

Fig. 7. Elastic nuclear breakup (dashed line) cross section $d\sigma/dE$ (in mb/MeV) for the reaction ^{17}F(65 MeV/nucleon) + Pb $\rightarrow$ ^{16}O + p + Pb, as a function of the proton–^{16}O relative energy, in MeV. The solid line includes the Coulomb breakup and the nuclear–Coulomb interference.

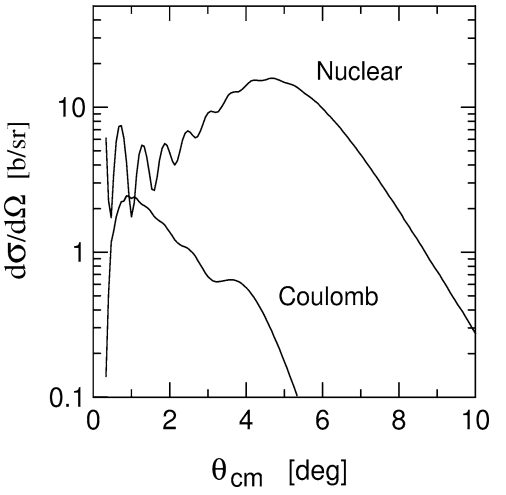

Fig. 8. Elastic nuclear breakup (upper curve) cross section $d\sigma/d\Omega$ (in b/sr) for the reaction ^{17}F(65 MeV/nucleon) + Pb $\rightarrow$ ^{16}O + p + Pb, as a function of the proton + ^{16}O center of mass scattering angle, in degrees. The lower curve line represents the Coulomb breakup contribution for the same reaction.

5. Conclusions

We have analyzed the possibility of using the reaction ^{17}F(65 MeV/nucleon) + Pb $\rightarrow$ ^{16}O + p + Pb for the purpose of studying the Coulomb reacceleration effects.

We have shown that the exclusive cross section is dominated by the elastic nuclear breakup. This shows that this reaction is not very useful for this purpose, even if the impact

parameter is selected by imposing an upper cut on the center of mass scattering angle. In this case, the contribution of the nuclear dissociation is reduced considerably, as shown in Ref. [26]. However, the Coulomb breakup cross section is also reduced. Since the total Coulomb breakup cross section only amounts to fractions of millibarns, we predict a very small counting rate for an experiment dedicated to this study.

Acknowledgements

This research was supported in part by the US National Science Foundation under Grants No. PHY-007091 and PHY-00-70818.

References

[1] G. Baur, C.A. Bertulani, H. Rebel, Nucl. Phys. A 458 (1986) 188.
[2] C.A. Bertulani, G. Baur, Nucl. Phys. A 442 (1985) 73.
[3] J. Kiener, A. Lefebre, P. Aguer, C.O. Bacri, R. Bimbot, G. Bogaert, B. Borderie, F. Claper, A. Coc, D. Disdier, S. Fortier, C. Grunberg, L. Klaus, I. Linck, G. Pasquier, M.F. Rivet, F. StLaurent, C. Stephan, L. Tassangot, J.P. Thibaud, Nucl. Phys. A 552 (1993) 66.
[4] J. Kiener, H.J. Gils, H. Rebel, S. Zagromski, G. Gsottschneider, N. Heide, H. Jelitto, J. Wentz, G. Baur, Phys. Rev. C 44 (1991) 2195.
[5] T. Motobayashi, et al., Phys. Lett. B 264 (1991) 259.
[6] A. Lefebre, et al., Nucl. Phys. A 595 (1995) 69.
[7] V. Tatischeff, J. Kiener, P. Aguer, A. Lefebvre, Phys. Rev. C 51 (1995) 2793.
[8] T. Motobayashi, N. Iwasa, Y. Ando, M. Kurokawa, H. Murakami, J. Ruan (Gen), S. Shimoura, S. Shirato, N. Inabe, M. Ishihara, T. Kubo, Y. Watanabe, M. Gai, R.H. France III, K.I. Hahn, Z. Zhao, T. Nakamura, T. Teranishi, Y. Futami, K. Furutaka, Th. Delbar, Phys. Rev. Lett. 73 (1994) 2680.
[9] T. Kikuchi, et al., Eur. Phys. J. A 3 (1998) 213.
[10] N. Iwasa, et al., Phys. Rev. Lett. 83 (1999) 2910.
[11] B. Davids, D.W. Anthony, T. Aumann, Sam M. Austin, T. Baumann, D. Bazin, R.R.C. Clement, C.N. Davids, H. Esbensen, P.A. Lofy, T. Nakamura, B.M. Sherrill, J. Yurkon, Phys. Rev. Lett. 86 (2001) 2750.
[12] B. Davids, D.W. Anthony, Sam M. Austin, D. Bazin, B. Blank, J.A. Caggiano, M. Chartier, H. Esbensen, P. Hui, C.F. Powell, H. Scheit, B.M. Sherrill, M. Steiner, P. Thirolf, Phys. Rev. Lett. 81 (1998) 2209.
[13] B. Davids, Sam M. Austin, D. Bazin, H. Esbensen, B.M. Sherrill, I.J. Thompson, J.A. Tostevin, Phys. Rev. C 63 (2001) 065806.
[14] J.N. Bahcall, Phys. Lett. B 433 (1998) 1.
[15] K. Langanke, T.D. Shoppa, Phys. Rev. 49 (1994) 1771.
[16] M. Gai, C.A. Bertulani, Phys. Rev. C 52 (1995) 1706.
[17] C.A. Bertulani, M. Gai, Nucl. Phys. A 636 (1998) 227.
[18] H. Esbensen, G. Bertsch, Nucl. Phys. A 600 (1996) 37.
[19] G. Baur, C.A. Bertulani, D.M. Kalassa, Nucl. Phys. A 550 (1992) 527.
[20] K. Ieki, et al., Phys. Rev. Lett. 70 (1993) 730.
[21] G.F. Bertsch, C.A. Bertulani, Nucl. Phys. A 556 (1993) 136;
G.F. Bertsch, C.A. Bertulani, Phys. Rev. C 49 (1994) 2834.
[22] H. Esbensen, G.F. Bertsch, C.A. Bertulani, Nucl. Phys. A 581 (1995) 107.
[23] F.M. Nunes, I.J. Thompson, Phys. Rev. C 59 (1999) 2652.
[24] R. Morlock, R. Kunz, A. Mayer, M. Jaeger, A. Mueller, J.W. Hammer, P. Mohr, H. Oberhummer, G. Staudt, V. Koelle, Phys. Rev. Lett. 79 (1997) 3837.
[25] J.F. Liang, et al., Phys. Lett. B 491 (2000) 23.
[26] H. Esbensen, G.F. Bertsch, Nucl. Phys. A 706 (2002) 383.

[27] F. Ajzenberg-Selove, Nucl. Phys. A 166 (1971) 1.
[28] B.A. Brown, A. Arima, J.B. McGrory, Nucl. Phys. A 277 (1977) 77.
[29] C.A. Bertulani, G. Baur, Nucl. Phys. A 480 (1988) 615.
[30] C.A. Bertulani, G. Baur, Phys. Rep. 163 (1988) 299.
[31] A.M. Kobos, B.A. Brown, R. Lindsay, G.R. Satchler, Nucl. Phys. A 425 (1984) 205.
[32] C.A. Bertulani, P. Lotti, H. Sagawa, Phys. Rev. C 57 (1998) 217.
[33] H. De Vries, C.W. De Jager, C. De Vries, At. Data Nucl. Data Tables 36 (1987) 495.
[34] C.A. Bertulani, A.M. Nathan, Nucl. Phys. A 554 (1993) 158.
[35] C.A. Bertulani, Nucl. Phys. A 587 (1995) 318.